The Effect of Membrane Thickness on a Microvascular Gas Exchange Unit

*Du T. Nguyen, Y T. Leho, and Aaron P. Esser-Kahn**

For reducing anthropogenic CO_2 emissions, carbon capture and sequestration technologies benefit from the creation of new and efficient gas exchange systems. Vascularized systems provide a means of exchanging CO_2 by providing high specific surface areas and patterned, intimate contact between capture fluids and gases. The well-defined geometrical arrangement of fluid and gas channels, separated by semipermeable membranes, also provides a new platform for augmenting the function of liquid chemical solutions to carbon capture. In particular, the separation distance of the channels, or polymer membrane thickness, is closely related to the absorption rate as gases must permeate through the membrane before reacting with a fluid. Here, a study of the relationship between the membrane thickness in 3D microvascular contactors and absorption rates via a selective etching process is reported. By decreasing the membrane thickness, the mass transport rate of CO_2 in the vascular contactor is increased by up to 160%.

1. Introduction

Each year, almost 29 billion metric tons of CO_2 are released into the atmosphere from anthropogenic sources.[1] This results in an atmospheric CO_2 concentration that is higher now than at any other point in history within the past 800 000 years.[2] These emissions are primarily caused by the combustion of fossil fuels which are expected to remain a primary source of energy production for the next 20 years.[3] As CO_2 is a major contributor to the global climate change, a route to lower emissions is required. Carbon capture and sequestration technologies (CCS) are being researched as a means of reducing CO_2 emissions from point sources such as power plants. In proposed CCS technologies, CO_2 is captured, compressed, transported, and stored in subterranean or submarine environments.[4] The U. S. Dept. of Energy has set a goal of achieving 90% CO_2 capture with the cost of energy increasing by no more than 35%.[5] The use of amine-based aqueous solutions such as monoethanolamine (MEA) is currently one of the most attainable methods of separating CO_2 from flue streams as they have already been used industrially for natural gas purification and food-grade CO_2 production.[6] However, using MEA is estimated to increase the cost of energy for a new plant by 80–85% and reduce the plant's efficiency by 30%, which hinders its widespread adoption.

Many low energy solutions using different chemistries have emerged as potential methods of capturing CO_2 from mixed gas streams including solid sorbents, new solvents, and membrane technologies.[7–15] In order for some of these solutions to be implemented at scales beyond the laboratory, they require larger, patterned structural platforms. However, very little research has been done in synthesizing these new platform materials. In nature, gas exchange is critical for survival and requires energy efficient systems. In contrast to current research, these natural systems use many different physical structures for gas exchange with very few different chemical methods. Inspired by nature, we are working towards the goal of building a platform analogous to the natural lung, a modular gas exchange system that has a low footprint, high-selectivity, and requires little energy.[16] Many methods have been developed to create vascular structures in soft materials for self-healing materials, tissue-growth, and autonomic cooling.[31] We have recently demonstrated the synthesis of biomimetic gas exchange units capable of capturing CO_2.[17] These gas exchange units are 3D arrays composed of hollow microchannels patterned within a polymer resin. The patterning of the channels creates short, polymer-filled separations that have many properties of the given polymer membrane. Our microvascular system also allows for the well-defined geometrical positioning of gases and fluids. We call these materials microvascular, based on their resemblance to natural structures. This microvascular design allows for high specific surface areas, which enhances the reactivity between capture fluids and gases. Furthermore, our microvascular structures can serve as a new platform for enhancing the larger scale function of emerging low-energy chemical solutions to carbon capture. Each microvascular unit is made with entirely commercially available components and can therefore be constructed in a scalable manner. In this report, we detail our effort to improve exchange rates and to better understand the relationship between the positions of individual channels in our material.

The microvascular gas exchange units were fabricated using the vaporization of a sacrificial component (VaSC) technique to create a 3D patterned microchannel structure.[18] This technique constructs arrays of microscale hollow channels within a polymer resin without lithography. The fabrication process is highly modular and allows for a wide range of both membrane materials and capture fluids. In this study, the units were

D. T. Nguyen, Y T. Leho, Prof. A. P. Esser-Kahn
University of California
Irvine, Irvine, CA 92697, USA
E-mail: aesserka@uci.edu

DOI: 10.1002/adfm.201201334

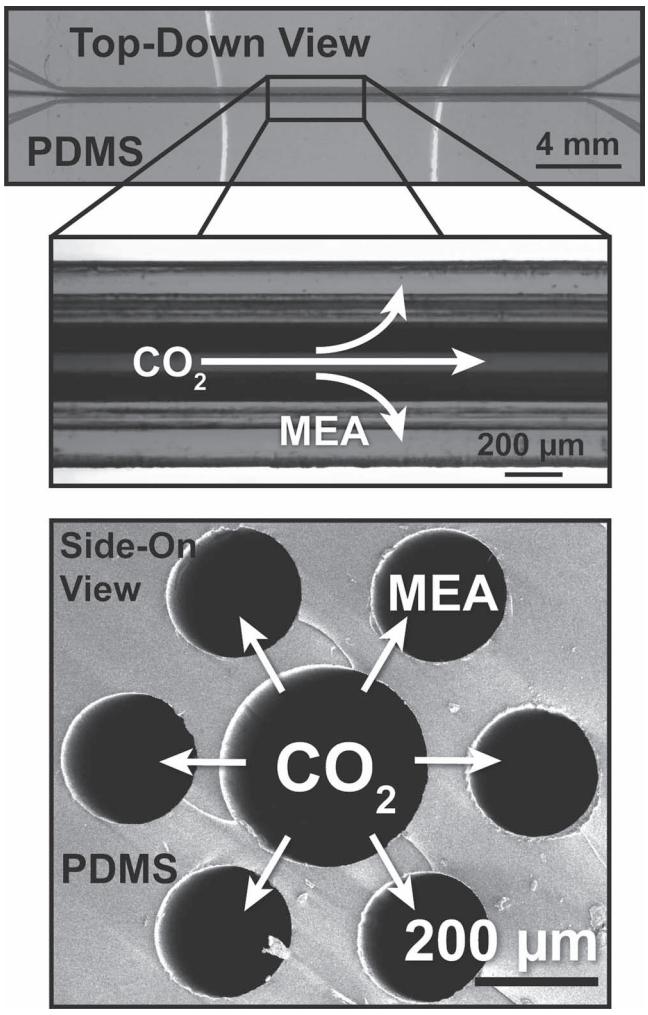

Figure 1. A representative gas exchange unit. Optical microscope and cross-sectional SEM images of a microvascular gas exchange unit composed of a central channel with a diameter of 300 µm and outer channels with diameters of 200 µm. The interchannel distance is initially 50 µm. Channels are separated in a second interface to ease the loading of channels with fluid and gas.

composed of a hexagonal arrangement of hollow channels embedded within polydimethylsiloxane (PDMS) as a model membrane. In each unit, the central channel began with a diameter of 300 µm while the outer channels had diameters of 200 µm. The separations between the central and outer channels started as 50 µm (**Figure 1**). This initial structure provided a specific surface area of 2267 m^2 m^{-3}. As a model capture-fluid, the industrial standard gas scrubbing liquid, 30% MEA in water, was loaded into the outer channels as CO_2 was flowed through the central channel. Upon entering the material, CO_2 permeated through the PDMS membrane until it reached the surface of the capture fluid channel. The CO_2 then reacted with the MEA at the surface and was subsequently retained as carbamic acid in the outer channels, completing the capture process.

In our microvascular gas exchange system, the interchannel distance was a critical parameter for controlling the permeability of CO_2 between the gas channel and the capture channel.

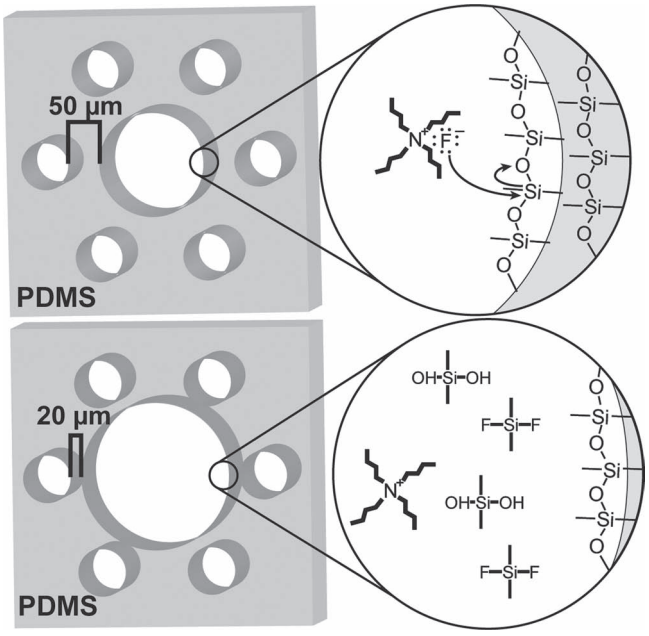

Figure 2. A schematic of the etching process. As TBAF flows through the central channel, the PDMS undergoes a nucleophilic attack from the fluoride anions. Through this process, the polymer sidewall is rapidly depolymerized. The products are cleared from the system as new etching solution is continually flowed into the channel. By etching the walls of the central channel, the interchannel distance is decreased between the central and outer channels.

A chemical etching technique was used to precisely modify the interchannel distance of a gas exchange unit as the distances dictated the thickness of the membrane.[19] A tetrabutylammonium fluoride (TBAF) in dimethylformamide (DMF) solution (3:1; vol:vol; DMF:75 wt% TBAF in water, hereafter referred to as the etching solution) was used to depolymerize the PDMS membrane of the exchange units (**Figure 2**). The fluoride anions in TBAF attacked the silicon centers of PDMS, forming Si-F bonds. The smooth laminar flow of the etching solution provided precise control over the etching rate. Upon removal of the PDMS, the central channel diameter increased causing the interchannel distance, or membrane thickness, to decrease. We confirmed the etching process by imaging horizontal and vertical cross-sections of the microchannels with a scanning electron microscope (SEM) (**Figure 3**). With this etching strategy, we were able to systematically study the relationship between membrane thicknesses and CO_2 capture rates. To simulate the gas exchange units, we have developed a computational finite element model which combines fluid flows, reaction rates, and diffusion rates. This model was able to accurately predict the capture rates in units with membrane thicknesses above 25 µm, but a divergence between the experimental results and the model occurred below such thicknesses. We further explore the divergence in this report.

2. Results and Discussion

To determine the etching rate of the process, samples were created with 500, 300, and 200 µm diameter channels. The etching

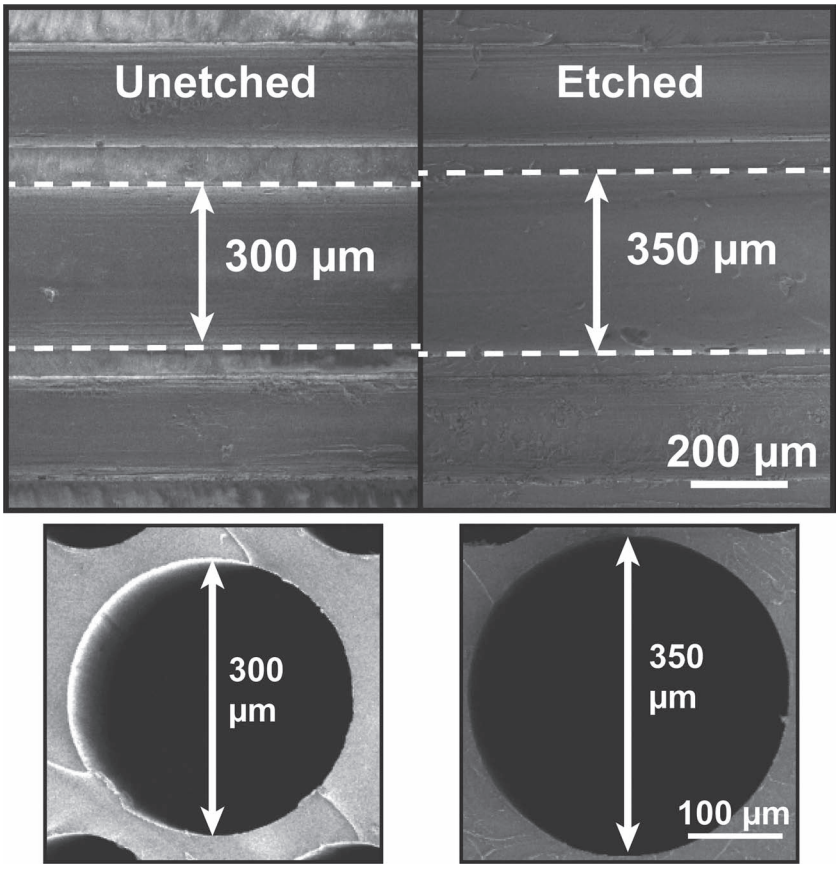

Figure 3. Visualization of etching. SEM images of a gas exchange unit taken before and after etching 50 µm of PDMS from the central microchannel. Both horizontal and vertical cross sections were imaged. The interchannel distance is decreased by 25 µm and results in higher mass transfer rates.

solution was flowed through the channels at a constant rate of 0.5 mL min^{-1} for 10 min. The channels were flushed with DMF at the same flow rate for 2 min to clear any remaining etching solution. A final rinse with 5 mL of DI water was then performed. While this resulted in different flow velocities for each channel due to the different channel radii, it provided an accessible calibration of the etching rate. The channel diameters were measured between each trial by imaging channels loaded with red dye for visualization. The channel diameters were computed with precise averages and errors using distance detection algorithms on the images across the entire length of the channels (Supporting Information). The overall etching rate for each initial channel diameter was calculated after multiple trials (**Figure 4**a). For the 200 and 300 µm channels, the etching rates were similar at ≈1 µm min^{-1} while the etching rate for the larger 500 µm channel was found to be ≈2 µm min^{-1}. Although only 300 µm diameter channels were etched in this study for the purpose of capturing CO_2, further optimization of the gas exchange units may use other initial channel diameters.

We also sought to understand the relationship between etching solution flow rates and etching rates. Samples were created with 500 µm diameter channels and etched at varying flow rates of etching solution for 5 min. The same flushing procedure with DMF and DI water was then performed on the samples. It was found that by increasing the flow rate, there was a slight increase of the etching rate which then levels off (Figure 4b). We believe this is due to the saturation of the fluoride ions at the surfaces of the channels above flow rates of 0.5 mL min^{-1}. Faster flow rates required more overall solution and provided negligible increases in the etching rate. This resulted in the use of lower flow rates to reduce the overall consumption of the etching solution.

With the calibration of the etching procedure prepared, we then sought to explore the effects of decreasing the interchannel distances on the ability of gas exchange units to capture CO_2. To determine the mass transfer rate of the units, a colorimetric technique was used. CO_2 was flowed through the central channel at a rate of 1 cm^3 min^{-1} while a solution of MEA (30:70, vol:vol, MEA:DI H_2O) was loaded into the outer channels. As MEA captures CO_2, the solution becomes more acidic (pH ≈12 to ≈8). This reaction was indirectly visualized by adding phenolphthalein, a pH sensitive dye that shifts color from red to colorless (red to light pink in bulk) once the channel was saturated with CO_2 (6 mg dye/mL MEA solution).[20] Defining the saturation time as 50% color change, the shift occurred at ≈9 wt% CO_2 (≈2.2 M carbamic acid) which was determined through UV-Vis spectroscopy (Supporting Information). This method allowed us to observe the reaction of CO_2 with MEA on an optical microscope in real time. Combining the saturation times with the saturation concentration, the average mass transfer rates could then be calculated.

The microvascular gas exchange units were also modeled using the COMSOL Multiphysics simulation software.[21] The model uses a combination of fluid flow and diffuse species transport physics to simulate the system. Several assumptions and parameters were used to create the model, including diffusion coefficients and reaction rates (Supporting Information). A time-dependent model was then created, simulating the flow and diffusion of CO_2 through a gas exchange unit as well as its reaction with MEA once it reached the outer channels. By averaging the concentration of carbamic acid over the outer channel volumes, we used the model to predict the saturation times for various interchannel distances (**Figure 5**). The model saturation times were defined as the time to reach 2.2 M carbamic acid and could then be compared with the experimental data. A linear trend of decreasing saturation times with decreasing channel separations was predicted.

Using this colorimetric technique, we determined the relationship between interchannel distances and gas exchange rates of our microvascular units with 100% CO_2. Between each trial, the central channel was etched for 4 min with an etching solution flow rate of 0.5 mL min^{-1} resulting in the interchannel distance decreasing by ≈4 µm per trial. The 3D arrangement of

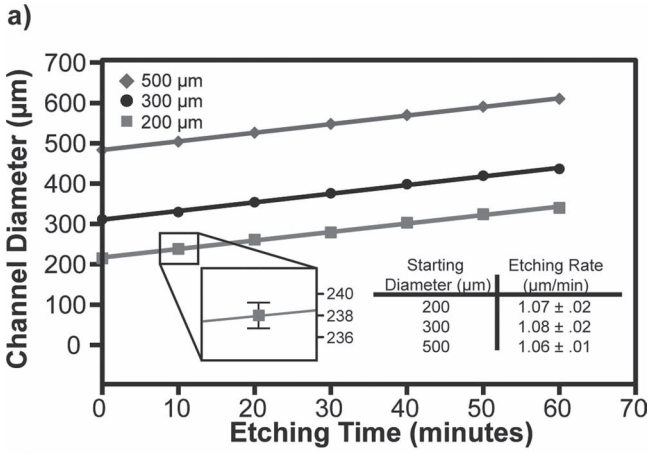

Flow Rate (mL min $^{-1}$)	Etching Rate (μm min^{-1})
2.00	1.07 ± .03
1.00	0.97 ± .02
0.50	1.06 ± .01
0.25	0.85 ± .03

Figure 4. Etching rate calibration. a) Etching rates for 500, 300, and 200 μm channel diameters with an etching solution flow rate of 0.5 mL min^{-1}. An enhanced set of a 200 μm channel is shown to illustrate error bars. b) Etching rates for varying etching solution flow rates in a 500 μm diameter channel. An increase in etching rate occurs as the flow rate increases.

channels interfered with the two-dimensional optical imaging of channels and resulted in large errors in the channel separation measurements. To reduce this error, MEA without dye was loaded into the upper and lower channels to increase transparency while the two flanking channels were loaded with dyed MEA for both the separation distance and saturation time measurements. The minimum membrane thickness reached was

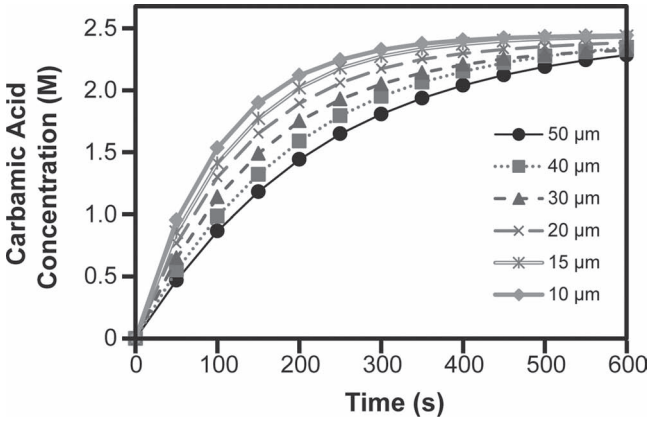

Figure 5. COMSOL model simulation of CO_2 capture in gas exchange units with various membrane thicknesses. As CO_2 diffuses into the outer channels, a reaction occurs with MEA, forming carbamic acid which is modeled by the software. The time to reach a concentration of ≈2200 mol m^{-3} is considered the saturation time.

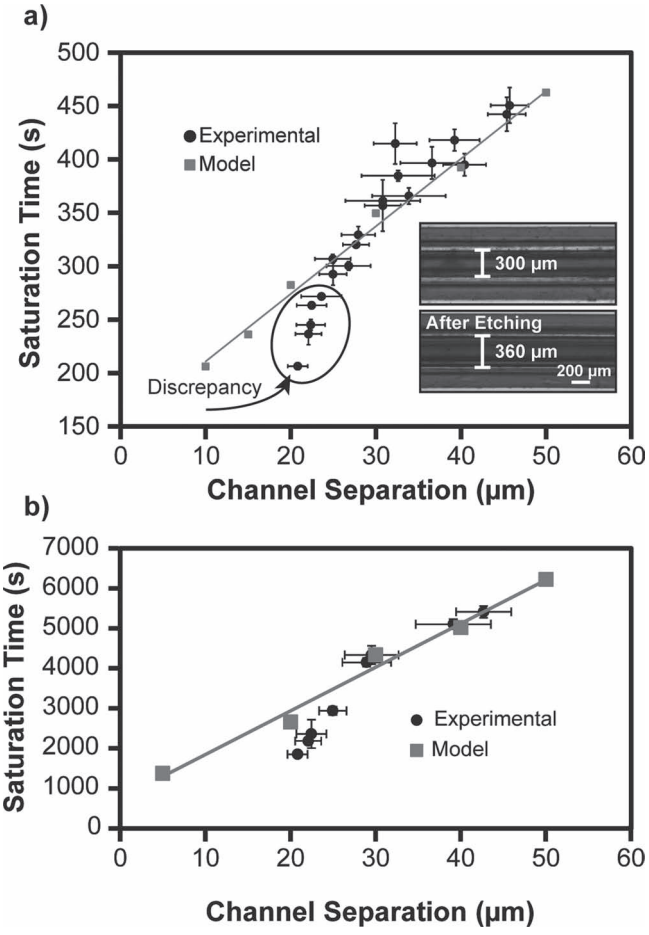

Figure 6. The effect of membrane thickness on saturation times. a) Saturation times for 100% CO_2. Inset is the channel before and after the etching trials were complete. Dye is loaded on the central and flanking outer channels while the upper and lower channels are loaded with water for visual clarity. b) Saturation times for 10 vol% CO_2 balanced with N_2. In both cases, as the membrane thickness decreases, the saturation times also decrease. Initially this trend is linear, but then accelerates and diverges from the model as the thickness decreases under 25 μm. The divergence is less prominent with the lower concentration of CO_2.

21 μm and resulted in a specific surface area of 2706 m^2 m^{-3}. As expected, the saturation times decreased when the interchannel distances decreased (**Figure 6**a). With thinner membranes, CO_2 diffused to the outer channels more rapidly. The initial gas exchange rate was found to be 3.59 ± 0.19 mol m^{-2} h^{-1} for an interchannel distance of 45.7 μm. For pure CO_2, the fastest mass transfer rate was found to be 6.86 ± 0.43 mol m^{-2} h^{-1} which was obtained for an interchannel distance of 20.8 μm. By etching the central channel to produce smaller interchannel distances, the mass transfer rate increased by 91%.

The experiment was repeated with a flue gas simulant of 10 vol% CO_2, balanced with N_2, to determine if the same trend would be found with lower concentrations of CO_2. The model again predicted a linear trend of decreasing saturation times with decreasing interchannel distances, and with saturation times increasing by a factor of 10 in comparison to using 100% CO_2. Again, a general decrease in saturation time with

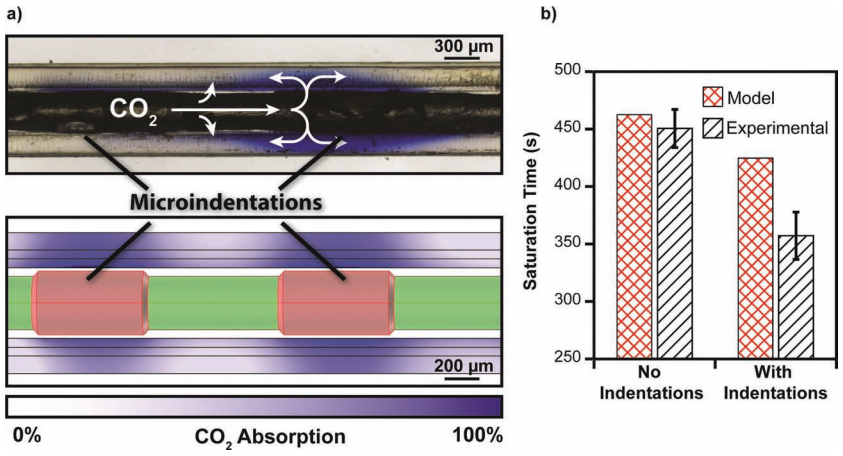

Figure 7. The effect of inducing microdents on the central channel. a) Experimental and model gas exchange units with microdents. Microdents are added to the model through additional cylindrical segments with larger radii than the central channel. Experimental microdents are added by fusing 25 µm PLA fibers to the central channel resulting in a rougher surface. b) A graph of saturation times with and without dents. In both cases with the microdents, a decrease in saturation time is observed. Only with the experimental data does this decrease in saturation time match the divergence from the model seen at low channel separations.

a decrease in membrane thickness was found (Figure 6b). The initial interchannel distance of 42.7 µm resulted in a mass transfer rate of 0.30 ± 0.02 mol m^{-2} h^{-1}. At the lowest interchannel distance of 20.8 µm, a mass transfer rate of 0.78 ± 0.03 mol m^{-2} h^{-1} was obtained, increasing by 160%. While this absolute rate may be lower in comparison to other devices such as hollow fiber membrane contactors (≈2 mol m^{-2} h^{-1}), the rates for other such devices include flowing rather than stationary MEA and slightly higher concentrations of CO_2 (≈14%).[22] This result suggests the intriguing possibility that creating gas exchange units with interchannel distances less than 20 µm could improve gas exchange rates more dramatically. However, we believe this may require a new approach to overall fabrication.

While the general trends with pure and 10% CO_2 matched our predictions, the linear trends expected by the model did not match with the experimental results. Instead, the trends were only linear at interchannel distances above ≈25 µm. When the distances were less than 25 µm, the saturation times decreased at a faster rate and diverged from the model. We attempted to decrease the interchannel distance below 20 µm, but were hindered by the leaking of capture fluid between the outer and central channels at various points along the channels. We examined what effects these leak points would have on the mass transfer rates to determine if they could cause the divergences. Leaking might be explained by the presence of microdents in the material prior to etching. The presence of these microdents creates membrane regions of smaller thicknesses. CO_2 could permeate through the membrane more rapidly at these points and then diffuse through the MEA solution resulting in a more rapid saturation time.

To understand if the divergences from the model at smaller interchannel distances were caused by microdents, we first attempted to model the system with simulated microdents. The microdents were simulated with cylindrical portions with 180 µm radii added to the central channel of the model with a 50 µm interchannel distance resulting in segments with closer separations. From the results of the model, the saturation time of a gas exchange unit with the microdents decreased by 25 s in comparison to the model with smooth channels (**Figure 7**). While this accounted for some of the discrepancy, the model did not fully agree with experiments. We then attempted to introduce microdents experimentally to examine the resulting decrease in saturation time. The microdents were created by joining extra PLA to the central channel using 25 µm fibers and TFE. With these artificially created microdents, the saturation time of a gas exchange unit with a 44 µm interchannel distance improved by ≈90 s. This rate was comparable to the divergence between the model and experimental saturation times at 20 µm separations. This result suggested that the microdents improved the mass transfer rates of a gas exchange unit and accounted for the divergences found previously. It also implied that smooth microchannels were not necessary to promote enhanced gas absorption rates in our microvascular gas exchange units.

3. Conclusions

We have demonstrated the ability to precisely control the interchannel distances of our microvascular gas exchange units at the microscale. This allows for the study of the connection between membrane thickness and gas exchange rates. Decreasing the membrane thickness resulted in increased mass transport. Below separations of ≈25 µm, the increase in mass transport with respect to the membrane thickness was further accelerated. The presence of microdents was found to be the cause of this acceleration and indicates that the entire interchannel membrane is not required to have uniform thickness to improve mass transfer rates. While we were unable to obtain interchannel distances below 20 µm due to the leakage of capture fluid between channels, membrane healing processes can potentially be used to repair the areas where leakage occurred and allow for channel separations below 20 µm.[23] Additionally, modifications to the surface chemistry of the channels may further enhance the reactivity of our microvascular gas exchange units. Also, it has not escaped our attention that PDMS is not an ideal material and we are interested in exploring alternative materials for synthesizing exchange units in future studies.

4. Experimental Section

Materials: Monoethanolamine (≥99%, MEA), phenolphthalein, methyl blue, tin (II) oxalate (98%) tetrabutylammonium fluoride solution (75 wt% in water, TBAF), and *N*,*N*-dimethylformamide (99.8%, DMF) were purchased from Sigma-Aldrich. Sylgard 184 silicone elastomer kit (PDMS) was purchased from Dow Corning. Disperbyk-130 was purchased from BYK Additives & Instruments. Trifluoroethanol (TFE) was purchased from Halogen Inc. Poly(lactic) acid (PLA) fibers were provided by Teijin Monofilament.

Preparation of Fibers for Exchange Unit Fabrication: PLA fibers were infused with tin (II) oxalate to lower its depolymerization temperature from 280 °C to 200 °C. A 800 mL treatment solution was created (400 mL deionized water, 400 mL trifluoroethanol, 50 g tin oxalate, 20 g DISPERBYK-130, 0.5 g malachite green) to infuse the tin oxalate within the fibers and to dye the fibers for visual clarity. Fibers were wound around a custom spindle and placed within the solution. The solution with the fibers was agitated by spinning the spindle at 300 RPM for 48 h at room temperature. The fibers were then removed from the solution and dried in air at room temperature for 24 h.

Gas Exchange Unit Fabrication: Gas exchange units were created using the Vaporization of a Sacrificial Component (VaSC) technique. Poly(lactic) acid (PLA) fibers were infused with a tin (II) oxalate (SnOx) catalyst. PDMS was created using mixtures of the Sylgard 184 silicone elastomer base and curing agent with a 10:1 ratio between base and curing agent. The mixture was then degassed using a rough vacuum pump and glass bell jar for 15 min. The fibers were strung through two laser-cut brass plates containing a hexagonal pattern. The plates were placed onto a mold box with the fibers tensioned on either side to create a set of parallel fibers in a hexagonal arrangement within the mold box. The mold box was then filled with PDMS and cured at 65 °C for 1 h. A second stage of molding with PDMS was performed to separate the channels from the hexagonal pattern and allow for easier loading of channels. The vascular preforms were heated to 210 °C under vacuum to vaporize and evacuate the fibers embedded within the PDMS resin resulting in the hexagonal arrangement of hollow channels.

Creating Microdents: A procedure similar to the fabrication of a normal gas exchange unit was followed. After the fibers were strung through the patterning plates, but before placement onto the mold box and tensioning, the microdents were added. Small loops of 25 µm PLA fibers were wrapped around the 300 µm central fiber. Single drops of TFE were added to the loops to meld the 25 µm fibers onto the central fiber. The remaining TFE was then dried in air and resulted in a central fiber with increased surface roughness to simulate the microdents.

COMSOL Model: To model the system, the Laminar Flow and Transport of Dilute Species modules were coupled to simulate the flow of CO_2, diffusion of CO_2, and reaction of CO_2 with MEA. Diffusion coefficients of 1.6×10^{-5} m^2 s^{-1}, 1.51×10^{-9} m^2 s^{-1}, and 7.08×10^{-10} m^2 s^{-1} for CO_2 in air, water, and PDMS respectively were used to determine the transport properties of the model.[24–26] The densities and dynamic viscosities of N_2 and CO_2 were used to determine the flow properties of 10 vol% CO_2 and 100% CO_2 respectively. The reaction rate between CO_2 and MEA was approximated using a first order reaction and calculated as $r = 6550[MEA]$ where r is the rate in mol m^{-3} s^{-1}.[27–30] Time-dependent simulations were run using a generalized alpha time-stepping method.

Optical Microscopy: Optical microscopy images were taken with a Zeiss Axio Observer.A1 Microscope at a 5× objective for determining interchannel distances and a 2.5× objective for determining saturation times. Tiled images were taken over the entire unit as water dyed with methyl blue was loaded into the central and flanking outer channels while water without dye was loaded into the upper and lower outer channels to determine the interchannel distances. To determine the saturation times, time-lapsed images with 4 s intervals were taken on marked central positions along the length of the gas exchange units. Regions of interest were made along the outer channels to quantify the image data within the regions. The average hue within the regions were found and normalized from the initial to final hue values. The time to reach 50% hue change was defined as the saturation time.

Scanning Electron Microscopy: SEM images were taken on a FEI Quanta FIB system (Oxford Instruments) with currents ranging from 1.06 pA to 4.74 pA and voltages ranging from 1.00 kV to 2.00 kV.

Supporting Information

Supporting Information is available from the Wiley Online Library or from the author.

Acknowledgements

This work was supported by the AFOSR Young Investigator Program under FA9550-12-1-0352 and a 3M Non-Tenured Faculty Award. The authors would like to acknowledge Lalisa Stutts and Janine Tom for helpful discussion relating to this project. The authors thank the Calit2 Microscopy Center and Laser Spectroscopy Facility at the University of California, Irvine for allowing use of its facilities. Hodge Harland and the UCI Physical Sciences Machine Shop are acknowledged for the fabrication of tools. The poly(lactic) acid fibers were generously provided by Teijin Monofilament.

Received: May 16, 2012
Published online: August 13, 2012

[1] P. Friedlingstein, R. A. Houghton, G. Marland, J. Hackler, T. A. Boden, T. J. Conway, J. G. Canadell, M. R. Raupach, P. Ciais, C. Le Quéré, *Nat. Geosci.* **2010**, *3*, 811.
[2] D. Lüthi, M. Le Floch, B. Bereiter, T. Blunier, J.-M. Barnola, U. Siegenthaler, D. Raynaud, J. Jouzel, H. Fischer, K. Kawamura, T. F. Stocker, *Nature* **2008**, *453*, 379.
[3] US. Energy Information Administration, *Annual Energy Outlook, 2011 with Projections to 2035* **2011**, Report # DOE/EIA-0383.
[4] H. J. Herzog, *Environ. Sci. Technol.* **2001**, *35*, 148A.
[5] U. S. Dept. of Energy, *Carbon Dioxide Capture from Existing Coal-Fired Power Plants* **2007**, Report # DOE/NETL-401/110901.
[6] J. P. Ciferno, T. E. Fout, A. P. Jones, J. T. Murphy, *Chem. Eng. Prog.* **2009**, *105*, 33.
[7] D. Britt, H. Furukawa, B. Wang, T. G. Glover, O. M. Yaghi, *Proc. Natl. Acad. Sci. USA* **2009**, *106*, 20637.
[8] H. Li, M. Eddaoudi, M. O'Keeffe, O. M. Yaghi, *Nature* **1999**, *402*, 276–279.
[9] J. D. Figueroa, T. Fout, S. Plasynski, H. McIlvried, R. D. Srivastava, *Int. J. Greenhouse Gas Control* **2008**, *2*, 9.
[10] R. Franchi, P. Harlick, A. Sayari, *Studies in Surface Science and Catalysis* Vol. 156 (Eds: A. Sayari, M. Jaroniec), Elsevier, Niagra Falls, Canada **2005**, pp. 879–886.
[11] R. A. Khatri, S. S. C. Chuang, Y. Soong, M. Gray, *Energy Fuels* **2006**, *20*, 1514.
[12] E. D. Bates, R. D. Mayton, I. Ntai, J. H. Davis, *J. Am. Chem. Soc.* **2002**, *124*, 926.
[13] D. Camper, J. E. Bara, D. L. Gin, R. D. Noble, *Ind. Eng. Chem. Res.* **2008**, *47*, 8496.
[14] R. P. Lively, R. R. Chance, B. T. Kelley, H. W. Deckman, J. H. Drese, C. W. Jones, W. J. Koros, *Ind. Eng. Chem. Res.* **2009**, *48*, 7314.
[15] I. C. Omole, R. T. Adams, S. J. Miller, W. J. Koros, *Ind. Eng. Chem. Res.* **2010**, *49*, 4887.
[16] J. N. Maina, S. A. Jimoh, M. Hosie, *J. Anat.* **2010**, *217*, 597.
[17] D. T. Nguyen, Y. T. Leho, A. P. Esser-Kahn, *Lab Chip* **2012**, *12*, 1246.
[18] A. P. Esser-Kahn, P. R. Thakre, H. Dong, J. F. Patrick, V. K. Vlasko-Vlasov, N. R. Sottos, J. S. Moore, S. R. White, *Adv. Mater.* **2011**, *23*, 3654.
[19] S. Takayama, E. Ostuni, X. Qian, J. C. McDonald, X. Jiang, P. LeDuc, M.-H Wu, D. E. Ingber, G. M. Whitesides, *Adv. Mater.* **2001**, *13*, 570.
[20] R. W. Sabnis, *Handbook of Acid-base Indicators*, CRC Press, Boca Raton, FL **2007.**
[21] Multiphysics Modeling and Simulation Software–COMSOL, 2012, http://www.comsol.com/(accessed July 2012).
[22] S. Yan, M.-X. Fang, W.-F. Zhang, S.-Y. Wang, Z.-K. Xu, Z.-Y. Luo, K.-F. Cen, *Fuel Process. Technol.* **2007**, *88*, 501.
[23] K. S. Toohey, N. R. Sottos, J. A. Lewis, J. S. Moore, S. R. White, *Nat. Mater.* **2007**, *6*, 581.

[24] D. T. Pritchard, J. A. Currie, *J. Soil Sci.* **1982**, *33*, 175.
[25] A. Tamimi, E. B. Rinker, O. C. Sandall, *J. Chem. Eng. Data* **1994**, *39*, 330.
[26] T. C. Merkel, V. I. Bondar, K. Nagai, B. D. Freeman, I. Pinnau, *J. Polym. Sci. Pol. Phys.* **2000**, *38*, 415.
[27] R. Maceiras, E. Álvarez, M. Á. Cancela, *Chem. Eng. J.* **2008**, *138*, 295.
[28] J. M. Plaza, D. V. Wagener, G. T. Rochelle, *Energy Procedia* **2009**, *1*, 1171.
[29] P. M. M. Blauwhoff, G. F. Versteeg, W. P. M. Van Swaaij, *Chem. Eng. Sci.* **1983**, *38*, 1411.
[30] R. Sakwattanapong, A. Aroonwilas, A. Veawab, *Energy Procedia* **2009**, *1*, 217.
[31] a) L. M. Bellan, S. P. Singh, P. W. Henderson, T. J. Porri, H. G. Craighead, J. A. Spector, *Soft Matter* **2009**, *5*, 1354; b) J. T. Borenstein, E. J. Weinberg, B. K. Orrick, C. Sundback, M. R. Kaazempur-Mofrad, J. P. Vacanti, *Tissue Eng.* **2007**, *13*, 1837; c) C. J. Hansen, W. Wu, K. S. Toohey, N. R. Sottos, S. R. White, J. A. Lewis, *Adv. Mater.* **2009**, *21*, 4143; d) J.-H. Huang, J. Kim, N. Agrawal, A. P. Sudarsan, J. E. Maxim, A. Jayaraman, V. M. Ugaz, *Adv. Mater.* **2009**, *21*, 3567; e) M. Shin, K. Matsuda, O. Ishii, H. Terai, M. Kaazempur-Mofrad, J. Borenstein, M. Detmar, J. P. Vacanti, *Biomed. Microdevices* **2004**, *6*, 269; f) B. D. Kozola, L. A. Shipton, V. K. Natrajan, K. T. Christensen, S. R. White, *J. Int. Mater. Sys. Struct.* **2010**, *21*, 1147; g) R. S. Trask, G. J. Williams, I. P. Bond, *J. R. Soc. Interface* **2007**, *4*, 363; h) L. M. Bellan, T. Kniazeva, E. S. Kim, A. A. Epshteyn, D. M. Cropek, R. Langer, J. T. Borenstein, *Adv. Healthcare Mater.* **2012**, *1*, 164; i) J. Lee, J. Paek, J. Kim, *Lab Chip* DOI:10.1039/c2l40267j; j) W. Wu, A. DeConinck, J. A. Lewis, *Adv. Mater.* **2011**, *23*, H178.